2012

Controlling calibration errors in gravitational-wave detectors by precise location of calibration forces

H. Daveloza
The University of Texas Rio Grande Valley

M Afrin Badhan

Mario C. Diaz
The University of Texas Rio Grande Valley

K. Kawabe

P. N. Konverski

See next page for additional authors

Controlling calibration errors in gravitational-wave detectors by precise location of calibration forces

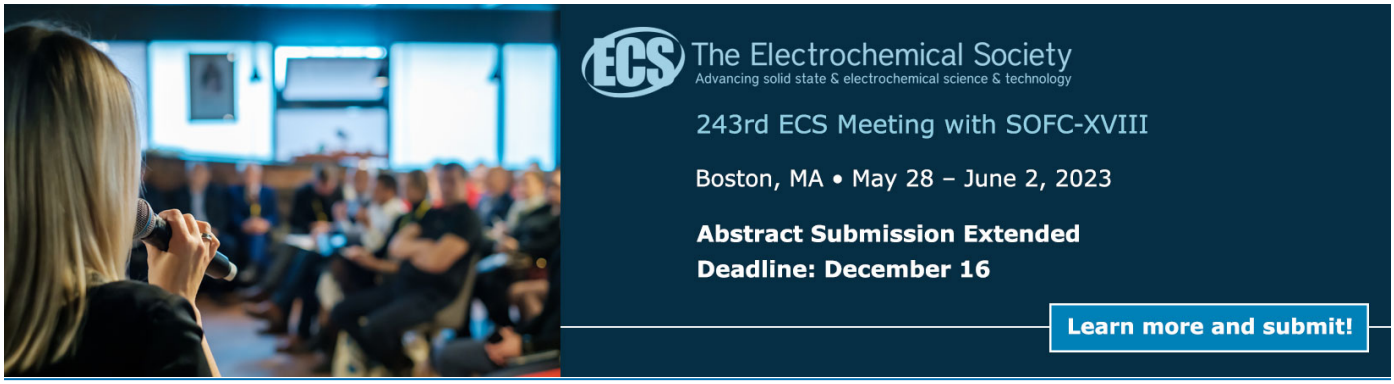

Journal of Physics: Conference Series **363** (2012) 012007 doi:10.1088/1742-6596/363/1/012007

Controlling calibration errors in gravitational-wave detectors by precise location of calibration forces.

H P Daveloza[1], M Afrin Badhan[2], M Diaz[1], K Kawabe[3], P N Konverski[1], M Landry[3] and R L Savage[3]

[1] Center for Gravitational Wave Astronomy, University of Texas at Brownsville, Brownsville, Texas, USA
[2] Mount Holyoke College, South Hadley, Massachusetts, USA
[3] LIGO Hanford Observatory, Richland, Washington, USA

E-mail: hernan.daveloza@ligo.org

Abstract. We present results of finite element analysis simulations which could lead to more accurate calibration of interferometric gravitational wave detectors. Calibration and actuation forces applied to the interferometer test masses cause elastic deformation, inducing errors in the calibration. These errors increase with actuation frequency, and can be greater than 50% at frequencies above a few kilohertz. We show that they can be reduced significantly by optimizing the position at which the forces are applied. The Advanced LIGO [1] photon calibrators use a two-beam configuration to reduce the impact of *local* deformations of the test mass surface. The position of the beams over the test mass can be chosen such both the local and the *bulk* induced elastic deformation are minimized. Our finite element modeling indicates that with two beams positioned within ± 1 mm of their optimal locations, calibration errors due to test mass elastic deformation can be kept below 1% for frequencies up to 3.5 kHz. We thus show that precise control of the location of calibration forces could considerably improve calibration accuracy, especially at high frequencies.

1. Introduction

Optimizing searches for gravitational wave sources at frequencies above 1 kHz [2] [3], will require improvements in the calibration of ground-based interferometric gravitational wave detectors. Lindblom has shown that optimizing scientific benefit requires calibration accuracies on the order of 5% for first detection and 0.5% for later measurements [4].

The Photon Calibrator (Pcal) is a calibration method that uses radiation pressure from auxiliary lasers to induce reference displacements of the interferometer's test masses. The Pcal has become one of the favored methods for determination of the interferometer's response function, due to its simplicity and ability to calibrate with forces that induce displacements that are close to what is expected from candidate Gravitational Wave (GW) sources. However, Hild et al. at GEO600 [5],

and Goetz et al. in LIGO [6] demonstrated that calibration forces exerted by the action of a centered Pcal beam produce local deformations that significantly change the sensed displacement at frequencies above about 500 Hz due to local elastic deformation of the test mass surface. Even though this type of local elastic deformation cannot be avoided, its effects can be mitigated by changing the configuration of the Pcal from one laser beam in the middle of the face of the test mass, to two laser beams diametrically opposed and sufficiently displaced from the center of the face such that local elastic deformations are not sensed by the interferometer. This scheme was tested and implemented in LIGO as part of the Enhanced LIGO upgrade [7] [8].

Willems [9] and Afrin Badhan et al. [10] studied another possible problem, the *bulk* elastic deformation of the End Test Masses (ETM). Their studies showed that these deformations also significantly impact the calibration accuracy, especially at high frequencies.

Our investigations show that actuation and calibration forces induce bulk deformations with spatial distributions given by the test mass normal mode shapes. The magnitude of the induced deformation increases dramatically as the frequency of excitation approaches the frequency of a given normal mode, affecting the interferometer length calibration. We incorporated the actual Initial LIGO ETM geometry and the actual physical parameters of the ETM (e.g. density, Young's modulus, Poisson's ratio, damping parameter or the inverse of the quality factor) into to our Finite Element Analysis. We also analyzed the elastic deformations of Advanced LIGO ETMs, predicting the deformations that would be produced by Pcal forces and identifying the optimal positions for the beams.

2. Elastic Theory

ETMs are made of fused silica. Although this is a stiff material, with a Young's modulus of 72.7 GPa and a Poisson's ratio of 0.16, they can experience small deformations when acted upon by calibration or actuation forces. For example, deformations on the order of 10^{-16} m induced by oscillating calibration forces of 10^{-8} N at a frequency of 3.5 kHz. Because the deformations are small, the response to the excitations induced by calibration forces can be represented with the appropriate linear combination of normal modes. We perform investigations to correctly identify these modes and their effects on the detector performance. As we will show, the amplitude in each mode, and then the deformation sensed by the interferometer, depends on the position of the calibration and actuation forces on the High-Reflective (HR) and Anti-Reflective (AR) surfaces of the ETMs.

The test masses of GW interferometers are right circular cylinders with one wedged flat surface. As introduced by Love [11], the first study of an ideal cylinder's elastic deformations was made by Pochhammer in 1876. Hutchinson, summarized these studies and presented a numerical method to calculate the normal modes of a solid cylinder [12].

GW interferometers measure the axial projection of the displacement of the surface of the test mass, $w = \vec{u} \cdot \vec{z}$, where $\vec{u}$ is the displacement vector and $\vec{z}$ is the direction parallel to the axis of the cylinder. Following Hutchinson, the solutions for this displacement are:

$$w = 2\delta J_n(\alpha r) \left\{ \begin{array}{c} -sin(\delta z) \\ cos(\delta z) \end{array} \right\} \cos(n\theta)$$

and

$$w = \alpha^2 J_n(\alpha r) \left\{ \begin{array}{c} -sin(\beta z) \\ cos(\beta z) \end{array} \right\} \cos(n\theta)$$

where J_n denotes the nth-order Bessel function and r, θ and z are the usual cylindrical coordinates. The numbers α, β and δ are related by $\alpha^2 + \delta^2 = (2\pi f)^2(1-2\nu)/2(1-\nu)$ and $\alpha^2 + \beta^2 = (2\pi f)^2$, where f is the frequency and ν is the Poisson's ratio.

The sensing by the main interferometer laser beam can be modeled as a Gaussian-weighted integral of the displacement over the entire HR surface. Due to the periodic azimuthal dependence ($cos(n\theta)$), the integrals for a centered interferometer beam will vanish except for the case of $n = 0$, in which case the azimuthal dependence vanishes. In this case we have a solution for w with only a Bessel dependence on the radial direction (the integral is performed over a surface, i.e. at $z = constant$). This mode is referred to as the *drumhead* mode.

We can reduce or eliminate the excitation of this mode by applying the forces at the nodes of this function. Associating the first minimum of $J_0(x)$ with the radius of the cylinder, a rough approximation for the ratio between the optimal radial position for the applied forces and the radius of the cylinder, is given by the ratio between the first root of $J_0(x)$ ($x \sim 2.40$), the first node, and the first root of its derivative ($x \sim 3.83$). The ratio is thus $2.40/3.83 = 0.63$.

Afrin Badhan et al. found a similar solution for the Initial LIGO ETMs and control system forces using Finite Element Analysis (FEA) [10]. To control the position of the ETM, Initial LIGO used four voice coil actuators with magnets glued to the AR surface of the ETM. Afrin Badhan modeled the ETMs as right circular cylinders of diameter $D = 250$ mm and thickness $\tau = 100$ mm with four forces applied uniformly over circles of 2 mm radius that are equally spaced displaced radially from the center of the AR surface. She found the optimum radius for the forces to be 82 mm, giving a ratio of 0.65.

The Initial LIGO ETMs are not perfect cylinders; the AR surface is wedge at 2 degree. In our analysis, see section 3 for more detail, we included this wedge and found the optimal radius to be 78.7 mm. The voice coil actuator were located at a radius of 114 mm, well outside the optimal position. Thus the contribution to the sensed motion arising from elastic deformation is in phase with the rigid body motion. The relative error, or discrepancy, in the overall sensed motion compared with the rigid body motion is plotted in Figure **1** for the actual position of the voice coil actuators (green squares) and for voice coil actuators located at the optimal radius (blue x's). For actuator at the Initial LIGO position, the induced error increases with frequency to a factor of 1.9 at 6 kHz. If the forces were located at the optimal radius, our analysis shows that the discrepancy would be less than one percent up to 6 kHz.

The measured discrepancy between the motion sensed by the interferometer and the expected free-mass motion, when the test mass is driven by the Initial LIGO voice coil actuators, has been observed [13] and is in reasonable agreement with the FEA results [10]. In order to maintain the accuracy of the interferometer calibration, the expected elastic deformation induced by the voice coil actuators must be, and is, included in the model of the interferometer response used for calibration [13].

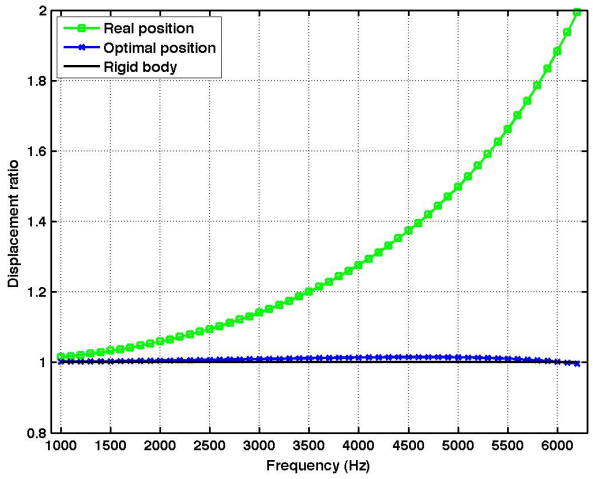

Figure 1

Ratio between total sensed motion and rigid-body motion vs. excitation frequency, for actual (114 *mm) and optimal* (78.7 *mm) calibration force positions.*

3. Finite Element Analysis

For this study we use COMSOL Multiphysics [14], a well known FEA software package. LIGO ETMs have thin dielectric film coatings to produce the HR and AR surfaces, which are not modeled in our FEA. The Initial LIGO ETM (iETM) have a diameter $D = 250.75$ mm, a maximum thickness $\tau = 99.63$ mm, and a 2° wedge on the AR surface. The voice coil actuators were modeled as four forces uniformly applied over circles of radius 2 mm equally spaced and displaced radially from the center of the AR surface. The Advanced LIGO End Test Masses (aETM) have $D = 340.13$ mm, $\tau = 200.2$ mm, a wedge of 0.077° on the AR surface, and two flats on the sides separated by 326.5 mm. The aETMs will use electrostatic drives [15] instead voice coil actuators.

LIGO ETMs are suspended as pendulums to isolate them from seismic noise. In our FEA models, we treat the ETMs as free bodies, a reasonable assumption for frequencies much larger than the ETMs pendulum resonance frequency, approximately 1 Hz. The total displacement of the HR surface is the combination of the free-mass motion and the displacement resulting from elastic deformation of the ETMs. The effective displacement measured by the interferometer is the overlap of this HR surface displacement with the main interferometer gaussian beam. The gaussian weighting for a centered interferometer beam is given by:

$$\frac{exp(-2(x^2+y^2)/r_{ifo}^2)}{2\pi \times r_{ifo}^2}$$

where the interferometer beam spot size, r_{ifo}, is 45 mm for the iETM, and 62 mm for the aETM. The denominator is a normalization factor.

Using the elastic theory described in Section 2, we analyzed the coupling from the actuation of the photon calibrator forces to the displacement of each mode. Our analysis shows that two normal

modes are most relevant for calibration frequencies below 6 kHz, the *butterfly* mode and the drumhead mode. The butterfly and drumhead mode resonant frequencies are 6612 Hz and 9221 Hz for the iETM, and 5953 Hz and 8151 Hz for the aETM, respectively. Figure **2** shows the deformation shape of the butterfly and drumhead mode for an aETM.

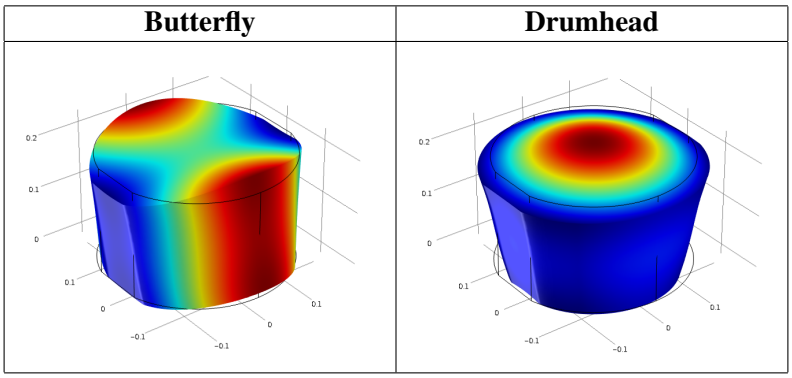

Figure 2
Advanced LIGO End Test Mass normal modes.

The drumhead mode has no azimuthal variation. The amplitude of the mode can be minimized by precise location of the actuation or calibration forces at the optimal radius, which is close to the nodal circle for the mode. The butterfly mode has a periodic variation with azimuthal angle. We already showed that for a perfect cylinder this periodic variation results in an effective zero displacement. Nevertheless, details of the actual test mass geometry, e.g. flats and wedges, affect the shapes and frequencies of the normal modes [16]. This is easy to visualize with *isosurfaces*; they are three dimensional surfaces with a constant value of the displacement of the elements. Figure **3** shows zero axial displacement *isosurfaces*, that is surfaces where $w = 0$, for an ideal cylinder and for an aETM.

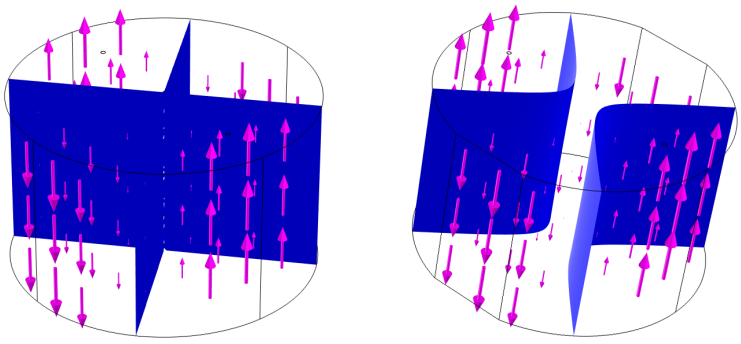

Figure 3
Butterfly mode $w = 0$ isosurfaces for an ideal cylinder (left) and an advanced LIGO End Test Mass (right). The arrows show the displacement vectors for the elements.

For ideal cylinders, the $w = 0$ isosurfaces cross the cylinder through its center, leaving an almost zero effective displacement. However, the $w = 0$ isosurfaces for the ETMs do not cross through the center of the cylinder, leaving an additional displacement that sums with the free-mass motion. Our study shows that the amplitude of the displacement produced by the elastic deformation for the butterfly mode can be minimized using three or four forces.

We also calculated the transfer function from photon calibrator forces to the displacement sensed by the interferometer to find an optimal placement of the photon calibrator beams. The Advanced LIGO Pcal forces were applied uniformly over circles of 2.5 mm radius, the approximate *spot size* for the laser beam. The discrepancy between the ideal rigid-body motion and the effective displacement measured by the interferometer is weakly dependent on the position of the interferometer beam, but strongly dependent on the positions of the driving forces. For frequencies below 4 kHz, the minimum discrepancy is observed when driving forces are positioned at 111.6 mm, giving a ratio between the optimal position and the aETM radius of 0.66. The resulting potential calibration errors are plotted versus excitation frequencies for a two-beam Pcal calibrator configuration in Figure **4**, and for a three-beam Pcal calibrator configuration in Figure **5**. For two optimally located beams the discrepancy is less than 0.1% up to 3.2 kHz and less than 1% for frequencies up to 4.3 kHz, but increases to almost 4% at 5 kHz.

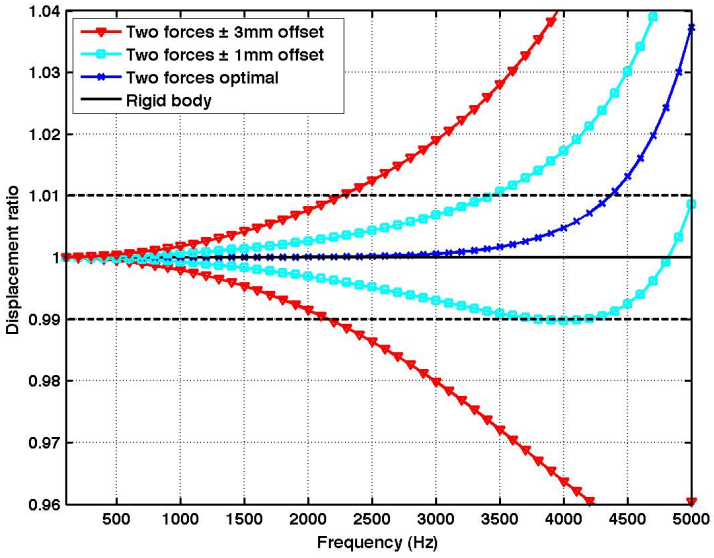

Figure 4

Advanced LIGO two-beams Photon calibrator configuration, ratio between total sensed motion and rigid-body motion vs. excitation frequency, for optimally positioned beams, 111.6 *mm, and* ± 1 *mm and* ± 3 *mm offsets from the optimal locations.*

The discrepancy increases dramatically for beams that are offset from their optimal positions. This increase in discrepancy for frequencies near and above 5 kHz can be understood by considering the increased compliance in the butterfly and drumhead deformation patterns as the excitation frequency approaches their resonance frequencies. The amplitude of the deformation

related to the butterfly mode is important only for frequencies close to it's resonant frequency, 6612 Hz for the iETM and 5953 Hz for the aETM, because far away from this frequencies the shape of this mode is governed by the azimuthal periodic variation that averages to zero for a centered interferometer beam. Thus, in general, the behavior of the discrepancy is governed by the amplitude of the elastic deformation related to the drumhead mode, because it directly involves the center of the ETMs with no periodic azimuthal dependence. For beams positioned in radius smaller than the optimal radius, the displacement produced by the drumhead mode is 180° out of phase with the free-mass motion, so these motion are subtracted. On the other hand, if the beams are positioned at a radius larger than the optimal radius, the displacement due to the drumhead mode is in phase with the free-mass motion and they add, so the discrepancy between the ideal rigid-body and the effective displacement always increases with frequency. Figure **4** shows this behavior. Note that above about 4 kHz, the ratio for Pcal beams positioned at radii smaller than the optimal radius, which initially decreased, begins to increase with frequency. This behavior, which is not observed for 3 forces, is due to excitation of the butterfly deformation pattern as the drive frequency approaches its resonance frequency.

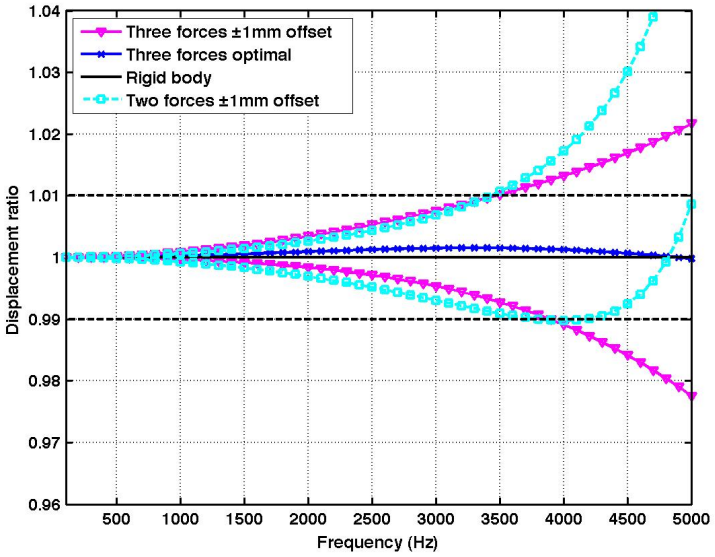

Figure 5

Advanced LIGO three-beam Photon calibrator configuration, ratio between total sensed motion and rigid-body motion vs. excitation frequency, for optimally positioned beams (112.7 mm) and ±1 mm offsets from the optimal locations.

If we now focus our attention to a discrepancy of 1%, we observe in Figure **4** that for an optimally positioned two-beam configuration this discrepancy is reached at 4.3 kHz. Meanwhile for an offset of 1 mm this discrepancy is reached at 3.5 kHz. In the case of three or four forces at the optimal radius, the discrepancy could be reduced to 0.2% for frequencies up to 5 kHz. Nevertheless, if the three or four forces are offset from the optimal locations by 1 mm, either intentionally or unintentionally due to poor positioning accuracy, the discrepancy is again 1% at 3.5 kHz, as can be

seen in Figure **5**. Thus, to realize the calibration accuracies called for in Lindblom's assessment, calibration forces must be localized within ± 1 mm of their optimal locations and multiple beam configurations will be required.

We also analyzed ETMs made of sapphire, a stiffer material than fused silica and a candidate material for future GW detectors test masses due to its increased thermal conductivity. For sapphire, normal modes moves to higher frequencies, butterfly ~ 9 kHz and drumhead ~ 14 kHz, resulting in, compared with fused silica, smaller deformation amplitudes for frequencies below 6 kHz which is desirable for GW detection and for high-frequency calibration accuracy.

We have also carried out a preliminary investigation of the electrostatic drives that will be used to control the aETMs [17]. Advanced LIGO's strict noise requirements demand that no magnets be glued to the ETMs, as was the case for Initial LIGO. The advanced LIGO suspension system, is a quadruple pendulum, in which the bottom masses are the ETMs and reaction masses are used to exert electrostatic forces on the ETMs via electrodes patterned on the reaction masses. Preliminary studies show that the electrostatic drives could produce calibration discrepancies of about 10% at 2.5 kHz and as much as 60% at 5 kHz due to the location of the forces.

4. Conclusions

Our analysis shows that actuation and calibration forces induce bulk deformations of test masses producing a discrepancy between the ideal free-mass, rigid-body motion and the effective displacement sensed by gravitational wave interferometers. The spatial distribution of these deformations are given by a superposition of the normal modes of the test mass with amplitudes that increase dramatically as the calibration or actuation excitation frequency approaches that of the normal modes. Even when the amplitude of the butterfly spatial deformation could be minimized using three or four forces, our study shows that, unless an accuracy of ± 1 mm in locating the calibration or actuation forces is achieved, there will be no advantage in using three or four forces for frequencies below 3.5 kHz. For an aETM with two Pcal beams positioned at a radius 111.6 ± 1.0 mm it is possible to keep the discrepancy between the ideal motion and the motion sensed by the interferometer below 1% up to 3.5 kHz. For frequencies above 3.5 kHz, calibration accuracy will be improved by adopting a Pcal configuration with three or more beams in order to minimize the amplitude of the butterfly bulk deformation pattern.

Acknowledgments

We thank P. Willems and the staff of the LIGO Hanford Observatory for enlightening discussions. We also thank the National Science Foundation for support under award HRD0734800. LIGO was constructed by the California Institute of Technology and Massachusetts Institute of Technology with funding from the National Science Foundation and operates under cooperative agreement PHY-0757058. This paper has LIGO Document Number LIGO-P1100166.

References

[1] Fritschel P, et al. 2009 Advanced LIGO Systems Design *LIGO document T010075* (https://dcc.ligo.org)
[2] LIGO Scientific Collaboration 2009 *Phy. Rev. D* **80** 102002.

[3] Maggiore M 2000 Stochastic backgrounds of gravitational waves (http://arxiv.org/abs/gr-qc/0008027v1)
[4] Lindblom L 2009 *Phy. Rev. D* **80** 042005.
[5] Hild S, et al. 2007 *Class. Quantum Grav.* **24** 5681-5688.
[6] Goetz E, et al. 2009 *Class. Quantum Grav.* **26** 245011.
[7] Abbott B, et al. 2009 *Rep. Prog. Phys.* **72** 076901 (http://iopscience.iop.org/0034-4885)
[8] Adhikari R, Fritschel P, Waldman S 2006 Enhanced LIGO *LIGO document T060156* (https://dcc.ligo.org)
[9] Willems P 2008 Finite Element Modeling of Test Mass Flexure Due to OSEM Forces *LIGO document T080190* (https://dcc.ligo.org)
[10] Afrin Badhan M, et al. 2009 Analyzing Elastic Deformation of Test Masses in LIGO *LIGO document T0900401* (https://dcc.ligo.org)
[11] Love A.E.H. 1944 A treatise on the mathematical theory of elasticity *Dover*
[12] Hutchinson J R 1980 *J. of Appl. Mech.* **47** 901-908.
[13] Bartos I, et al. 2011 Frequency Domain Calibration Error Budget for LIGO in S6 *LIGO document T1100071* (https://dcc.ligo.org)
[14] www.comsol.com
[15] M. Hewitson, H. Grote, G. Heinzel, K. A. Strain, H. Ward, U. Weiland 2003 *Class. Quantum Grav.* **20** S885-S893.
[16] Miller J, et al. 2011 *Phys. Lett. A* **375** 788-794.
[17] Daveloza H, et al. 2011 aLIGO Photon Calibrator Errors due to Elastic Deformation *LIGO document G1100332* (https://dcc.ligo.org)